Acta Crystallographica Section B
Structural Science
ISSN 0108-7681

Crystal structure of the high-pressure phase of the oxonitridosilicate chloride $Ce_4[Si_4O_{3+x}N_{7-x}]Cl_{1-x}O_x$, $x \simeq 0.2$

Alexandra Friedrich,[a]* Eiken Haussühl,[a] Wolfgang Morgenroth,[b] Alexandra Lieb,[c] Björn Winkler,[a] Karsten Knorr[d] and Wolfgang Schnick[c]

[a]Institut für Geowissenschaften, Abt. Kristallographie, Johann Wolfgang Goethe-Universität Frankfurt, Senckenberganlage 30, D-60054 Frankfurt a. M., Germany, [b]Mineralogisch-Petrologisches Institut, Poppelsdorfer Schloß, Universität Bonn, D-53115 Bonn, Germany, [c]Department Chemie und Biochemie, Lehrstuhl für Anorganische Festkörperchemie, Ludwig-Maximilians-Universität München, Butenandtstraße 5-13 (D), D-81377 München, Germany, and [d]Institut für Geowissenschaften, Christian-Albrechts Universität zu Kiel, Olshausenstraße 40, D-24098 Kiel, Germany

Correspondence e-mail: friedrich@kristall.uni-frankfurt.de

Received 10 September 2005
Accepted 26 January 2006

The structural compression mechanism of $Ce_4[Si_4O_{3+x}N_{7-x}]Cl_{1-x}O_x$, $x \simeq 0.2$, was investigated by *in situ* single-crystal synchrotron X-ray diffraction at pressures of 3.0, 8.5 and 8.6 GPa using the diamond–anvil cell technique. On increasing pressure the low-pressure cubic structure first undergoes only minor structural changes. Between 8.5 and 8.6 GPa a first-order phase transition occurs, accompanied by a change of the single-crystal colour from light orange to dark red. The main structural mechanisms, leading to a volume reduction of about 5% at the phase transition, are an increase in and a rearrangement of the Ce coordination, the loss of the Ce2, Ce3 split position, and a bending of some of the inter-polyhedral Si—N—Si angles in the arrangement of the corner-sharing Si tetrahedra. The latter is responsible for the short *c* axis of the orthorhombic high-pressure structure compared with the cell parameter of the cubic low-pressure structure.

1. Introduction

The oxonitridosilicates represent a link between oxosilicates and nitridosilicates (Schnick, 2001), as the Si atoms are surrounded by O and N atoms. Like nitridosilicates and oxonitridoaluminosilicates they show high chemical and thermal stability as well as mechanical hardness (Hampshire, 1994; Thompson & Mandal, 1996; Nordberg *et al.*, 1998). However, little is known about the high-pressure stability of oxonitridosilicates and the pressure dependence of the coordination polyhedra in this class of compounds. Initial theoretical studies based on quantum-mechanical density-functional theory pointed towards a possible pressure-induced phase transition of $Ce_4[Si_4O_4N_6]O$ (Winkler *et al.*, 2001). The high-pressure properties of isotypic oxonitridosilicate chlorides $Ce_4[Si_4O_{3+x}N_{7-x}]Cl_{1-x}O_x$, $x = 0.12$ and 0.18, were reported from powder synchrotron X-ray diffraction (Friedrich *et al.*, 2005). These compounds are related to the end-member $Ce_4[Si_4O_4N_6]O$ (Irran *et al.*, 2000) by a combined substitution of nitrogen for oxygen within the $Si(N,O)_4$ tetrahedra and of chlorine for oxygen (Lieb *et al.*, 2005). The ambient-pressure crystal structure of $Ce_4[Si_4O_{3+x}N_{7-x}]Cl_{1-x}O_x$, $x \simeq 0.2$, exhibits a layer of Q^3-type connected $SiON_3$ and SiN_4 tetrahedra (Lieb *et al.*, 2005). Within the layer the tetrahedra form three-membered rings, which are cross-linked through additional tetrahedra. The topology of the layer is 'hyperbolically corrugated' (Irran *et al.*, 2000) and this is the origin of the unexpected cubic symmetry for a Q^3-type connected silicate. The cavities within this tetrahedral network are filled by $[Ce_4Cl_{1-x}O_x]^{(11-x)+}$ cation groups (Fig. 1). The high-pressure experiments on powder samples revealed a reversible first-

Table 1
Experimental details.

Pressure (GPa)	3.0	8.5	8.6
Crystal	*A*	*B*	*B*
Crystal data			
Chemical formula	$Ce_4Cl_{0.92}N_{6.92}O_{3.16}Si_4$	$Ce_4Cl_{0.93}N_{6.93}O_{3.14}Si_4$	$Ce_4Cl_{0.93}N_{6.93}O_{3.14}Si_4$
M_r	853.05	853.28	853.28
Cell setting, space group	Cubic, $P2_13$	Cubic, $P2_13$	Orthorhombic, $P2_12_12_1$
Temperature (K)	293 (2)	293 (2)	293 (2)
a, b, c (Å)	10.347 (4), 10.347 (4), 10.347 (4)	10.223 (3), 10.223 (3), 10.223 (3)	10.824 (9), 10.479 (3), 8.967 (3)
V (Å^3)	1107.8 (7)	1068.4 (5)	1017.1 (10)
Z	4	4	4
D_x (Mg m^{-3})	5.115	5.305	5.572
Radiation type	Synchrotron	Synchrotron	Synchrotron
Radiation wavelength (Å)	0.45	0.45	0.45
No. of reflections for cell parameters	10	20	16
θ range (°)	3.7–11.9	4.4–12.7	3.1–9.9
μ (mm^{-1})	4.48	4.65	4.89
Crystal form, colour	Plate-like, orange	Round plate, orange	Round plate, red
Crystal size (mm)	0.60 × 0.15 × 0.10	0.11 × 0.11 × 0.04	0.11 × 0.10 × 0.04
Data collection			
Diffractometer	HUBER diffractometer, D3, HASYLAB/DESY	HUBER diffractometer, D3, HASYLAB/DESY	HUBER diffractometer, D3, HASYLAB/DESY
Data collection method	ω scan, continuous, fixed φ method	ω scan, continuous, fixed φ method	ω scan, continuous, fixed φ method
Scan steps, width (°), time per step (s)	61, 0.003, 0.4–0.8	61, 0.004, 0.4–0.8	61, 0.03, 0.4–0.8
Absorption correction	Gaussian	Gaussian	Gaussian
T_{min}	0.360	0.377	0.404
T_{max}	0.482	0.507	0.503
No. of measured, independent and observed reflections	1712, 476, 471	1557, 535, 510	1726, 823, 663
Criterion for observed reflections	$I > 2\sigma(I)$	$I > 2\sigma(I)$	$I > 2\sigma(I)$
R_{int}	0.051	0.042	0.084
θ_{max} (°)	14.0	15.4	15.0
Range of h, k, l	$-10 \Rightarrow h \Rightarrow 10$ $-8 \Rightarrow k \Rightarrow 10$ $-6 \Rightarrow l \Rightarrow 10$	$-12 \Rightarrow h \Rightarrow 11$ $-12 \Rightarrow k \Rightarrow 12$ $-8 \Rightarrow l \Rightarrow 6$	$-8 \Rightarrow h \Rightarrow 4$ $-12 \Rightarrow k \Rightarrow 12$ $-10 \Rightarrow l \Rightarrow 10$
No. and frequency of standard reflections	1 every 50 min	1 every 50 min	1 every 50 min
Refinement			
Refinement on	F^2	F^2	F^2
$R[F^2 > 2\sigma(F^2)]$, $wR(F^2)$, S	0.024, 0.063, 1.02	0.028, 0.070, 1.04	0.054, 0.122, 1.06
No. of reflections	476	535	823
No. of parameters	37	37	79
Weighting scheme	$w = 1/[\sigma^2(F_o^2) + (0.0375P)^2 + 16.083P]$, where $P = (F_o^2 + 2F_c^2)/3$	$w = 1/[\sigma^2(F_o^2) + (0.0449P)^2 + 11.8113P]$, where $P = (F_o^2 + 2F_c^2)/3$	$w = 1/[\sigma^2(F_o^2) + (0.0676P)^2]$, where $P = (F_o^2 + 2F_c^2)/3$
$(\Delta/\sigma)_{max}$	0.019	0.074	<0.0001
$\Delta\rho_{max}$, $\Delta\rho_{min}$ (e Å^{-3})	0.90, −0.86	1.35, −1.26	1.55, −1.98
Extinction method	*SHELXL*	*SHELXL*	None
Extinction coefficient	0.0067 (8)	0.0030 (8)	–

Computer programs used: *DIF*4 (Eichhorn (1987*a*), *REDUCE* (Eichhorn, 1987*b*), *AVSORT* (Eichhorn 1978), *ABSORB*, v6.0 (Angel, 2004), *SHELXS*97 (Sheldrick, 1997*a*), *SHELXL*97 (Sheldrick, 1997*b*), *ATOMS* (Dowty, 1999).

order phase transition between 8 and 10 GPa with noticeable hysteresis (Friedrich *et al.*, 2005). The pressure at which the phase transition occurs is dependent on composition. The transition is characterized by a change of symmetry from $P2_13$ to $P2_12_12_1$ following a *translationengleiche* group–subgroup relationship, and a volume reduction of $\sim 5\%$ (Friedrich *et al.*, 2005). While compressibilities of both phases were obtained from these data, no information on the structural compression mechanism or the crystal structure of the high-pressure phase could be derived. The aim of the present study is to clarify the pressure dependence of the crystal structure above and below the phase-transition pressure. The results of this study will contribute to a better understanding of the structural mechanisms occurring at the phase transition.

2. Experimental

Syntheses of single crystals of end-member compositions were not successful. While the use of CsCl as a flux medium enhanced the formation of single crystals compared with pure $Ce_4[Si_4O_4N_6]O$, the $Ce_4[Si_4O_3N_7]Cl$ end-member did not seem to be stable under the conditions of the syntheses, as a small amount of oxygen (10–20%) was always incorporated into the chlorine site. Hence, single crystals were always obtained of

Table 2
Selected inter-atomic distances (Å), polyhedral volumes V (Å^3) and inter-polyhedral angles (°) for cubic $Ce_4[Si_4O_{3+x}N_{7-x}]Cl_{1-x}O_x$, $x \simeq 0.2$.

p (GPa)	0.0001†	3.0	8.5
Ce1—O3/N3*a*	2.308 (5)	2.279 (9)	2.251 (9)
Ce1—O1	2.510 (4)	2.483 (6)	2.440 (6)
Ce1—O3/N3*a*	2.537 (6)	2.518 (8)	2.515 (9)
Ce1—N2	2.603 (7)	2.561 (9)	2.57 (1)
Ce1—N1	2.600 (7)	2.58 (1)	2.55 (1)
Ce1—N2	2.633 (7)	2.62 (1)	2.61 (1)
Ce1—Cl/O2	2.982 (2)	2.941 (3)	2.907 (3)
V	25.85 (5)	25.04 (7)	24.25 (8)
Ce2—Cl/O2	1.99 (3)	1.95 (3)	1.94 (3)
Ce2—N1	2.556 (9) 3×	2.53 (1) 3×	2.45 (1) 3×
TQE‡	1.051 (3)	1.051 (4)	1.058 (4)
V	6.81 (2)	6.54 (3)	6.02 (3)
Ce2—Ce3	1.22 (3)	1.22 (3)	1.15 (3)
Ce3—O3/N3*a*	2.561 (6) 3×	2.555 (9) 3×	2.54 (1) 3×
Ce3—N1	2.599 (6) 3×	2.57 (1) 3×	2.51 (1) 3×
Ce3—Cl/O2	3.208 (4)	3.169 (5)	3.089 (5)
V	23.45 (7)	22.8 (1)	21.8 (1)
Si1—O3/N3*a*	1.689 (6)	1.681 (9)	1.662 (9)
Si1—N1	1.718 (6)	1.69 (1)	1.67 (1)
Si1—N2	1.709 (7)	1.70 (1)	1.69 (1)
Si1—N1	1.738 (7)	1.73 (1)	1.74 (1)
TQE‡	1.010 (5)	1.010 (9)	1.008 (9)
V	2.54 (1)	2.49 (2)	2.44 (2)
Si2—O1	1.66 (1)	1.63 (1)	1.63 (1)
Si2—N2	1.696 (7) 3×	1.70 (1) 3×	1.67 (1) 3×
TQE‡	1.000 (8)	1.00 (1)	1.00 (1)
V	2.46 (1)	2.42 (2)	2.34 (2)
Si1—N1—Si1	122.0 (4)	122.6 (6)	122.0 (7)
Si2—N2—Si1	157.2 (5)	155.6 (6)	158.3 (7)
Cl/O2—Ce1	2.983 (2) 3×	2.941 (3) 3×	2.907 (3) 3×
Cl/O2—Ce2	1.99 (3)	1.95 (3)	1.94 (3)
Cl/O2—Ce3	3.208 (4)	3.169 (5)	3.087 (5)
TQE (Ce1,Ce2) ‡	1.045 (6)	1.048 (6)	1.054 (6)
V (Ce1,Ce2)	10.20 (6)	9.71 (5)	9.31 (5)
TQE (Ce1,Ce3) ‡	1.027 (2)	1.031 (2)	1.040 (2)
V (Ce1,Ce3)	13.86 (1)	13.23 (1)	12.45 (1)

† Ambient pressure; data were taken from Lieb *et al.* (2005). ‡ The tetrahedral quadratic elongation (TQE) is given after Robinson *et al.* (1971) and was calculated using the program *VOLCAL* (Finger, 1971).

the composition $Ce_4[Si_4O_{3+x}N_{7-x}]Cl_{1-x}O_x$, $x \simeq 0.2$ (Lieb *et al.*, 2005). The chemical composition was determined by several different quantitative analyses (Lieb *et al.*, 2005).

Two samples (crystal *A*: 150 × 100 × 60 µm^3; crystal *B*: 112 × 105 × 35 µm^3) were pressurized using ETH-type diamond–anvil cells (Miletich *et al.*, 2000). Holes of 220 µm in diameter, serving as pressure chambers, were drilled through steel gaskets (pre-indented to a thickness of 100 µm) using a spark-eroding drilling machine. A mixture of methanol and ethanol (4:1) served as a pressure-transmitting medium. Pressures were determined by means of the laser-induced ruby-fluorescence technique (Mao *et al.*, 1978).

In situ high-pressure single-crystal synchrotron X-ray diffraction was performed at the bending-magnet beamline D3 at HASYLAB. Intensity data were collected on a HUBER four-circle diffractometer using a point detector and a wavelength of 0.45 Å provided by a Si(111) double-crystal monochromator. The intensity measurements were carried out with ω scans according to the fixed φ technique (Finger & King, 1978) in order to select the beam path of least attenuation through the pressure cell. All accessible reflections within half an Ewald sphere and at $\varphi = 0°$ were collected in ω scan mode up to $2\theta \simeq 30°$. Data were collected at 3.0 GPa (crystal *A*) and 8.5 GPa (crystal *B*) for the cubic low-pressure phase and at 8.6 GPa (crystal *B*) for the high-pressure phase. Although the reflections from the high-pressure phase were broad and weak, the orthorhombic unit cell is in excellent agreement with the unit cell previously determined from powder X-ray diffraction data (Friedrich *et al.*, 2005; Table 1). For each pressure the appropriate scan parameters were selected (Table 1).

Intensity data were obtained from the scan data by the Lehmann–Larsen algorithm implemented in the beamline-specific software *REDUCE* (Eichhorn, 1987*b*), and corrected for Lorentz and polarization effects as well as intensity drifts of the primary beam (*AVSORT*; Eichhorn, 1978). The absorption of the X-ray beam by the sample, the diamonds and beryllium plates of the pressure cell was corrected using the program *ABSORB* (Angel, 2004). Structure solution and refinements were carried out with *SHELXS*97-2 and *SHELXL*97-2, respectively (Sheldrick, 1997*a*,*b*), with the starting parameters for the refinements of the cubic phases being taken from the structural data published by Lieb *et al.* (2005). The structure of the high-pressure orthorhombic phase was solved using direct methods and completed by difference-Fourier analyses. The final refinements of the high-pressure data sets were carried out with isotropic displacement parameters for all atoms, except for the Ce2/3 site in the high-pressure phase at 8.6 GPa, which was refined with anisotropic displacement parameters. The displacement parameters of the individual species occupying a split site (see below) were set to be equal. For mixed sites, a single atomic displacement parameter was used. Atoms occupying Wyckoff sites 12(*b*) in the cubic structure are each related to three symmetrically independent positions on Wyckoff sites 4(*a*) in the orthorhombic structure. The respective sites are labelled by the suffix *A*, *B* and *C*. The displacement parameters of the N2*A*, N2*B* and N2*C* atoms were set to be equal and the displacement parameter of the N1*B* atom was constrained to be that of N1*C* at

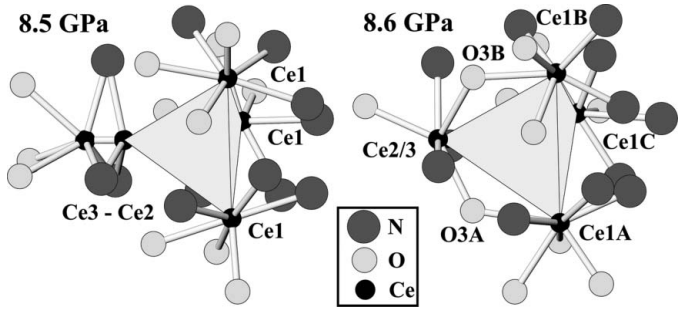

Figure 1
Coordination of the Ce cations and the $[Ce_4Cl_{0.93}O_{0.07}]^{10.93+}$ cation group, which is drawn as a tetrahedron with Cl and O as central atoms, at 8.5 GPa (left) and 8.6 GPa (right). At 8.5 GPa the tetrahedron is only drawn to one of the split sites, namely to the Ce2 site. Si atoms are not drawn. Abbreviations of atom labels: O3*A* ≡ O3*A*/N3*aA* and O3*B* ≡ O3*B*/N3*aB*.

Table 3
Selected inter-atomic distances (Å), polyhedral volumes V (Å^3) and inter-polyhedral angles (°) for orthorhombic $Ce_4[Si_4O_{3+x}N_{7-x}]Cl_{1-x}O_x$, $x \simeq 0.2$ at 8.6 GPa.

Ce1*A*—O3*B*†	2.28 (4)	Ce1*B*—O3*C*†	2.33 (6)	Ce1*C*—O3*A*†	2.33 (5)	Ce2/3—O3*C*†	2.55 (4)
Ce1*A*—O1	2.40 (4)	Ce1*B*—O1	2.56 (2)	Ce1*C*—O1	2.45 (3)	Ce2/3—O3*A*†‡	2.48 (3)
Ce1*A*—O3*A*†	2.71 (4)	Ce1*B*—O3*B*†	2.57 (4)	Ce1*C*—O3*C*†	2.77 (2)	Ce2/3—O3*B*†‡	2.68 (3)
Ce1*A*—N2*C*	2.52 (4)			Ce1*C*—N2*A*	2.43 (5)	Ce2/3—N1*B*	2.45 (4)
Ce1*A*—N1*B*	2.41 (4)	Ce1*B*—N1*C*	2.33 (6)	Ce1*C*—N1*A*	2.86 (3)	Ce2/3—N1*C*	2.48 (3)
Ce1*A*—N2*A*	2.64 (7)	Ce1*B*—N2*C*	2.43 (3)	Ce1*C*—N2*B*	2.58 (3)	Ce2/3—N1*A*	3.00 (5)
Ce1*A*—Cl/O2	2.93 (1)	Ce1*B*—Cl/O2	2.95 (1)	Ce1*C*—Cl/O2	2.79 (2)	Ce2/3—Cl/O2	2.88 (1)
Ce1*A*—O3*C*†	2.64 (2)	Ce1*B*—N1*A*	2.66 (3)	Ce1*C*—N2*B*	2.50 (5)		
V	28.9 (5)		23.1 (4)		28.3 (4)		24.8 (4)
Si1*A*—O3*A*†	1.63 (5)	Si1*B*—O3*B*†	1.65 (2)	Si1*C*—O3*C*†	1.68 (2)	Si2—O1	1.65 (3)
Si1*A*—N1*B*	1.74 (6)	Si1*B*—N1*C*	1.73 (4)	Si1*C*—N1*A*	1.70 (6)	Si2—N2*C*	1.65 (7)
Si1*A*—N2*A*	1.69 (3)	Si1*B*—N2*C*	1.71 (5)	Si1*C*—N2*B*	1.72 (3)	Si2—N2*B*	1.71 (5)
Si1*A*—N1*A*	1.73 (3)	Si1*B*—N1*B*	1.71 (6)	Si1*C*—N1*C*	1.71 (5)	Si2—N2*A*	1.73 (3)
TQE§	1.02 (3)	–	1.01 (3)	–	1.01 (7)	–	1.01 (6)
V	2.45 (9)	–	2.5 (1)	–	2.49 (8)	–	2.40 (8)
Cl/O2—Ce1*C*	2.79 (2)	–	Si1*C*—N1*C*—Si1*B*	117 (4)	Si2—N2*C*—Si1*B*	141 (3)	–
Cl/O2—Ce1*A*	2.93 (1)	–	Si1*A*—N1*A*—Si1*C*	122 (3)	Si2—N2*B*—Si1*C*	157 (4)	–
Cl/O2—Ce1*B*	2.95 (1)	–	Si1*B*—N1*B*—Si1*A*	121 (2)	Si2—N2*A*—Si1*A*	135 (2)	–
Cl/O2—Ce2/3	2.88 (1)						
TQE§	1.03 (1)						
V	11.88 (6)						

† O3*A* ≡ O3*A*/N3*aA*, O3*B* ≡ O3*B*/N3*aB*, O3*C* ≡ O3*C*/N3*aC*. ‡ The bond is not equivalent to that of the low-pressure phase in Table 2 (see Fig. 1). § The tetrahedral quadratic elongation (TQE) is given after Robinson *et al.* (1971) and was calculated using the program *VOLCAL* (Finger, 1971).

8.6 GPa. The Ce2:Ce3, Cl:O2 and O3:N3*a* site-occupancy ratios were refined for the cubic structures by coupled substitutions while maintaining charge neutrality. In the high-pressure structure the O3*A*:N3*aA*, O3*B*:N3*aB*, O3*C*:N3*aC* and Cl:O2 site occupancies were fixed to the refined O3:N3*a* and Cl:O2 ratios at 8.5 GPa. A unit-cell setting with $a > b > c$ was chosen for the orthorhombic high-pressure structural model in order to have the atomic coordinates comparable to those of the cubic structure. Experimental details and crystal data are summarized in Table 1.

3. Results and discussion

Atom positions, displacement parameters and site-occupancy factors have been deposited into the IUCr electronic archives.[1] Inter-atomic distances, polyhedral volumes and selected inter-polyhedral angles are listed in Table 2 for the low-pressure phase and in Table 3 for the high-pressure phase.

The pressures determined by the ruby fluorescence technique correspond, within 0.1 GPa, to the pressures obtained from the unit-cell volumes (p = 3.1, 8.6 and 8.5 GPa, respectively) by applying the equations of state which were previously determined for $Ce_4[Si_4O_{3+x}N_{7-x}]Cl_{1-x}O_x$, x = 0.12 and 0.18 (Friedrich *et al.*, 2005). The unit-cell volumes at ambient pressure were taken from the given equations of state, as the composition of the examined single crystals is assumed to be similar to that of the powder samples. For a detailed comparison, the cell parameter at ambient pressure was determined to be a = 10.446 (1) Å from in-house single-crystal X-ray diffraction and a = 10.4294 (1) Å from in-house powder X-ray diffraction (Lieb *et al.,* 2005). From powder synchrotron X-ray diffraction data, cell parameters of a = 10.433 (2) Å and a = 10.426 (1) Å were determined for the compositions with x = 0.12 and x = 0.18, respectively (Friedrich *et al.*, 2005).

3.1. Cubic low-pressure phase

3.1.1. Site-occupancy factors and disorder. In the cubic structure of both the Cl-free end-member $Ce_4[Si_4O_4N_6]O$ and the Cl-rich $Ce_4[Si_4O_{3+x}N_{7-x}]Cl_{1-x}O_x$, $x \simeq 0.2$, compound one of the Ce cations was modelled by split positions (Ce2 and Ce3), which are both located on special sites on the threefold axes such as the Cl/O2 site (Fig. 1; Irran *et al.*, 2000; Lieb *et al.*, 2005). The Ce3 site, which is located ∼ 1.22 (3) Å further away from the Cl/O2 site than the Ce2 site (Table 2, Fig. 1), seems to be increasingly occupied with increasing Cl concentration (Lieb *et al.*, 2005). This correlation can be confirmed within the accuracy of our data, which are in very good agreement with the data reported by Lieb *et al.* (2005). The good quality of the high-pressure data at 3.0 GPa (crystal *A*) and at 8.5 GPa (crystal *B*) allowed the refinement of the occupancy ratios to Ce2:Ce3 ≃ 0.040 (2):0.960 (2) and Cl:O2 ≃ 0.925 (4):0.075 (4). However, the real error of the refined occupancies is larger. A comparison with electron probe microanalyses [Cl = 86 (5 ≡ 2σ)%; Lieb *et al.*, 2005] leads to an assumed Cl content between 80 and 90%. The introduction of the split site leads to an unreasonably short Ce2—Cl/O2 distance of 1.99 (3) Å (Table 2). This problem can be solved by assuming additional disorder effects on the surrounding O and Cl/O2 positions. Such disorder has been already described for $Ce_4[Si_4O_4N_6]O$ by Irran *et al.* (2000), where 65–83% of the Ce2 positions are populated. In the present study no diffuse scattering has been observed. The implied disordered oxygen positions cannot be

[1] Supplementary data for this paper are available from the IUCr electronic archives (Reference: BK5022). Services for accessing these data are described at the back of the journal.

resolved from our data due to the low occupancy of the disordered positions. We assume that the actual coordination of Ce2 is sevenfold as in $Ce_4[Si_4O_4N_6]O$ (Irran *et al.*, 2000).

3.1.2. Compression of the crystal structure. The compression of the crystal structure of the cubic phase proceeds up to 8.5 GPa mainly by bond shortening as symmetry restrains the changes of inter-tetrahedral angles. While the distance between the Ce2 and Ce3 sites does not change up to 3.0 GPa, it is slightly reduced towards 8.5 GPa (Table 2). The most pronounced changes are observed within the $[Ce_4Cl_{0.93}O_{0.07}]^{10.93+}$ cation group (Fig. 1). The (Cl,O)Ce_4 tetrahedral volume is strongly reduced with increasing pressure, which is mainly achieved by a shortening of the Ce2—Cl/O2 and Ce3—Cl/O2 bonds along the threefold axes, respectively (Table 2). Further, the tetrahedral quadratic elongation, which was calculated according to Robinson *et al.* (1971), increases noticeably with increasing pressure (Table 2).

The $SiON_3$ and SiN_4 tetrahedra form relatively stiff polyhedral units similar to the SiO_4 units in most silicates (Hazen & Finger, 1982). Our data do not allow a reliable calculation of the tetrahedral compressibilities. Hence, we cannot comment on the influence of the covalence of bonding in these tetrahedra with respect to SiO_4 tetrahedra on the high-pressure properties.

3.2. The phase transition

As discussed previously in Friedrich *et al.* (2005), the high-pressure phase transition is reversible and shows hysteresis. The volume reduction is quite large, approximately 5%. The occurrence of a discontinuity in the volume evolution accompanied by hysteresis is characteristic for a phase transition of first order.

3.2.1. Twinning. The reduction of symmetry from $P2_13$ to $P2_12_12_1$ at the phase transition, as observed by Friedrich *et al.* (2005), has been confirmed. Following a *translationengleiche* group–subgroup relationship of index 3 the threefold axes are lost at the phase transition, which is classified as a proper ferroelastic phase transition (Stokes & Hatch, 1988). According to group theory the total number of domains in the low-symmetry form can be obtained by dividing the number of symmetry elements in the high-symmetry phase by the number of symmetry elements in the low-symmetry phase (Salje, 1990). Hence, three domains, or three different orientations of the orthorhombic cell with respect to the cubic cell, may exist. The occurrence of twinning was checked with an in-house kappa four-circle diffractometer (XCalibur3, Oxford Diffraction) equipped with a CCD camera. Two domains were unambiguously identified and indexed properly. The domains were rotated by $\sim 233^\circ$ around the (pseudo) threefold rotation axis [111]. The rotation angle differs by $\sim 7^\circ$ from the ideal angle of 240°. This difference is likely due to the large spontaneous deformation of the orthorhombic unit cell with respect to the cubic metric.

After the phase transition the reflections from one of the two domains dominated the scattering pattern. Consequently, only intensities of these reflections were measured with the point detector and used for the structure determination. The transformation matrix from this component to the twin domain was

$$\begin{pmatrix} 0.0025 & 1.0259 & 0.0070 \\ 0.1661 & -0.0117 & 1.1549 \\ 0.8197 & -0.0004 & -0.1689 \end{pmatrix}.$$

In the ideal case of a threefold rotation axis the corresponding transformation matrix would be

$$\begin{pmatrix} 0 & 1 & 0 \\ 0 & 0 & 1 \\ 1 & 0 & 0 \end{pmatrix}.$$

The transformation matrix from the main component to the third possible domain would be expected to be near to

$$\begin{pmatrix} 0 & 0 & 1 \\ 1 & 0 & 0 \\ 0 & 1 & 0 \end{pmatrix}.$$

Owing to the strong distortion of the crystal lattice, no pseudo-merohedral twinning is expected. The reflections of the two domains found are supposed to be well separated, especially for the high-resolution synchrotron X-ray beam. An inspection of the individual reflections confirmed that no peak splitting occurs. An evaluation of the CCD data collected at the laboratory X-ray source showed that reflection classes $(hk\bar{k})$ and (hkl) with $k + l = 6$ of domain one are close to reflection classes $(hk\bar{h})$ and (hkl) with $h + l = 6$ of domain two (if referring to the setting with $a > b > c$). A significant influence on the crystal structure refinement due to overlapping reflections, however, can be excluded. This was probed by adding the relevant reflections to the refinement of the orientation matrix – the metric of the twin domain changed significantly from the correct values. Furthermore, the refinement of the intensity data did not improve when the possibly affected reflections or only the few reflections along the twin axis were omitted. Hence, all the arguments led to the conclusion that no correction for partial reflection overlap from twin components is necessary for the data of the high-pressure phase.

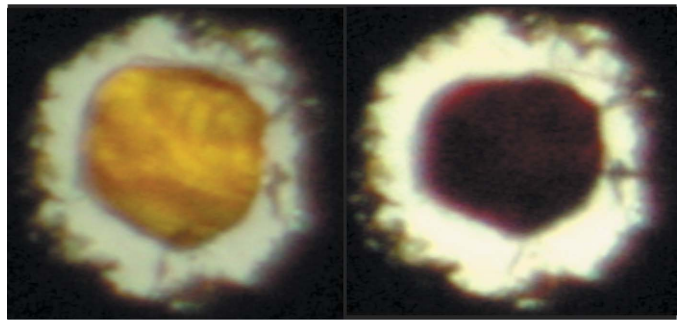

Figure 2
Single crystal of $Ce_4[Si_4O_{3+x}N_{7-x}]Cl_{1-x}O_x$, $x \simeq 0.2$, within the pressure chamber (crystal *B*, ~ 110 µm diameter). The crystal colour changes from light orange for the low-pressure phase (8.5 GPa; left side) to dark red for the high-pressure phase (8.6 GPa; right side).

The reflections from the high-pressure phase are broader and less intense than those from the low-pressure cubic phase. The broadening seems to be due to the evolution of smaller coherent domains in the low-symmetry phase as a result of the phase transition. The decrease in intensity can be explained by the division of the scattering volume into at least two domains in the high-pressure phase. This reduces the overall data quality compared with the low-pressure data and explains the higher internal residual value.

3.2.2. Optical behaviour. At the phase transition between 8.5 and 8.6 GPa we observed a spontaneous change of the single-crystal colour from transparent light-orange (in the low-pressure phase) to nearly opaque dark red (in the high-pressure phase; Fig. 2). The optical quality of the single crystal is reduced in the high-pressure phase, which might be due to the occurrence of several smaller domains as described above. After pressure release, the transparency and light-orange colour of the low-pressure phase is regained while the morphology remains intact.

3.3. Crystal structure of the orthorhombic high-pressure phase

The volume reduction at the phase transition is due to an increase in and a rearrangement of the coordination of the large Ce cations, as well as a bending of some inter-polyhedral Si—N—Si angles, associated with a rotation of the Si(O, N)$_4$ tetrahedra.

The coordination of the Ce cations, which occupy the cavities within the anionic Si(O, N)$_4$ tetrahedral arrangement, changes significantly. Owing to the loss of the threefold axes, three different Ce1 sites (Ce1*A*, Ce1*B*, Ce1*C*) exist that are equivalent in the cubic low-pressure structure (Fig. 3). While the Ce1 cation is sevenfold coordinated by O, N and Cl in the cubic structure, Ce1*A* and Ce1*C* are eightfold coordinated, forming an additional Ce1*A*—O3*C* and Ce1*C*—N2*B* bond, respectively. Ce1*B* is still sevenfold coordinated with a different arrangement of the nearest neighbours. A new Ce1*B*—N1*A* bond is formed, while a Ce1*B*—N2*B* bond is broken (Table 3, Fig. 3). The Ce1*B* polyhedral volume is reduced at the phase transition, while the volumes of the Ce1*A* and Ce1*C* polyhedra are increased due to the increase of the coordination. In the orthorhombic high-pressure structure the distance between the split Ce2 and Ce3 positions approaches ~ 0.3 Å. This justifies a refinement of a single Ce2/3 position. However, the isotropic displacement factor of this site is increased compared with those of the Ce1*A*, Ce1*B* and Ce1*C* sites. A refinement with anisotropic displacement parameters results in an elongated displacement ellipsoid along the direction of the former split position. The compression of the Ce2/3 polyhedron mainly affects the bond distance between the large Ce and Cl ions, reducing the polyhedral volume of the $[Ce_4Cl_{0.93}O_{0.07}]^{10.93+}$ cation group (Table 3). Here, again, two Ce3—O3/N3*a* bonds are broken and two new bonds (Ce2/3—O3*A*/N3*aA* and Ce2/3—O3*B*/N3*aB*) are formed. It is suggested that these new bonds are already part of the actual Ce2 coordination in the disordered cubic low-pressure structure, as is the case for $Ce_4[Si_4O_4N_6]O$. The changes in coordination are illustrated in Fig. 1.

The Si(O, N)$_4$ tetrahedral volumes do not change at the phase transition within their standard deviations (Tables 2 and 3). The main change within the tetrahedra connectivity at the phase transition is expressed in a variation of inter-polyhedral Si—N—Si angles (Fig. 4). While the Si1—N1—Si1 angle does not change during the loss of the threefold axes within its standard deviation, the Si2—N2—Si1 angle behaves differently in different directions, exhibiting a strong reduction of two of the related angles from 158 (1)° to 141 (3)° and 135 (2)°

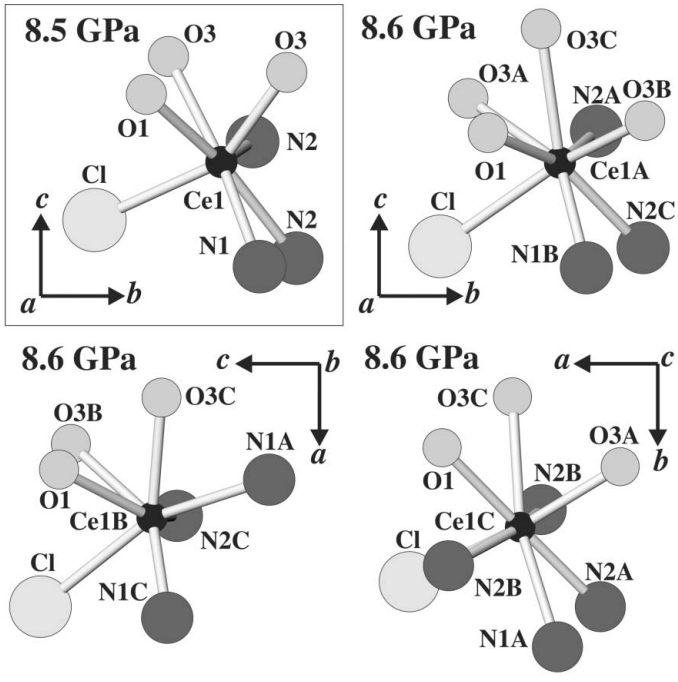

Figure 3
Coordination in the Ce1 polyhedron at 8.5 GPa and the Ce1*A*, Ce1*B* and Ce1*C* polyhedra at 8.6 GPa. Si atoms are not drawn. Abbreviations of atom labels: O3 ≡ O3/N3*a*, O3*A* ≡ O3*A*/N3*aA*, O3*B* ≡ O3*B*/N3*aB*, O3*C* ≡ O3*C*/N3*aC*, Cl ≡ Cl/O2.

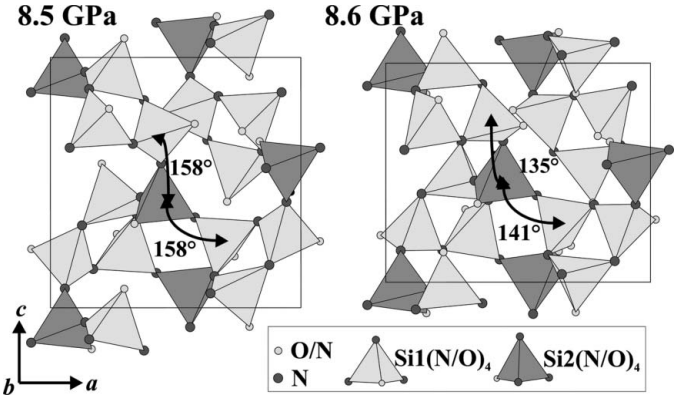

Figure 4
Projection of the Si(N,O)$_4$ tetrahedral arrangement of the cubic low-pressure phase of $Ce_4[Si_4O_{3+x}N_{7-x}]Cl_{1-x}O_x$, $x \simeq 0.2$, at 8.5 GPa and of the orthorhombic high-pressure phase at 8.6 GPa. The strong bending of some inter-polyhedral Si—N—Si angles is also shown. Ce atoms and the mixed Cl/O2 positions are not drawn.

towards Si1*A* and Si1*B*, respectively (Tables 2 and 3). This rotation of $Si(O, N)_4$ tetrahedra is accompanied by a rotation of the $(Cl,O)Ce_4$ tetrahedra within the cavities of the $Si(O, N)_4$ tetrahedral network. The reduction of inter-polyhedral Si—N—Si angles and, hence, rotation of the $Si(O, N)_4$ and $(Cl,O)Ce_4$ tetrahedra leads to the strong anisotropic compression of the cubic structure at the phase transition and results in the short *c* dimension of the orthorhombic phase (Fig. 4).

4. Summary

This is the first high-pressure single-crystal X-ray diffraction study of an oxonitridosilicate framework structure consisting of corner-connected $Si(O, N)_4$ tetrahedra. The present experiments on $Ce_4[Si_4O_{3+x}N_{7-x}]Cl_{1-x}O_x$, $x \simeq 0.2$, allowed us to suggest a model for the mechanism of the high-pressure phase transition, which was previously observed from powder X-ray diffraction (Friedrich *et al.*, 2005). The general compression behaviour shows a strong similarity to that in oxosilicates (compare *e.g.* Hazen & Finger, 1982). The main mechanism of volume reduction during the phase transition is by the change of inter-tetrahedral angles of the relatively rigid $Si(O, N)_4$ tetrahedra. As a result of that deformation the effective coordination of the cerium cations is modified and, hence, the crystal field. Most probably this alters the optical properties as expressed by the unusually strong change of the single-crystal colour. Further high-pressure X-ray absorption and luminescence spectroscopy experiments are being performed in order to probe to what extent a change of the electronic properties of cerium occurs at the phase transition and may possibly cause the observed colour change.

The authors gratefully acknowledge financial support from the Deutsche Forschungsgemeinschaft (DFG) through two grants (WI 1232/17-1 and SCHN 377/9) within the project SPP-1136, and from the Fonds der Chemischen Industrie, Germany. Thanks are due to the HASYLAB for synchrotron beam time. The authors appreciate the use of the high-pressure laboratory of H. Ahsbahs, University of Marburg, and his helpful advice, and the provision of a fully equipped ETH diamond–anvil cell by R. Miletich, University of Heidelberg.

References

Angel, R. J. (2004). *J. Appl. Cryst.* **37**, 486–492.
Dowty, E. (1999). *ATOMS*5.0. Shape Software, 521 Hidden Valley Road, Kingsport, TN 37663, USA.
Eichhorn, K. (1978). *AVSORT*, modified 1995. HASYLAB/DESY, Hamburg, Germany.
Eichhorn, K. (1987*a*). *DIF*4, modified 1995. HASYLAB/DESY, Hamburg, Germany.
Eichhorn, K. (1987*b*). *REDUCE*, modified 1995. HASYLAB/DESY, Hamburg, Germany.
Finger, L. W. (1971). *VOLCAL*. Carnegie Institute of Washington, Geophysics Laboratory, Washington DC, USA.
Finger, L. W. & King, H. E. (1978). *Am. Mineral.* **63**, 337–342.
Friedrich, A., Knorr, K., Lieb, A., Rath, St., Hanfland, M., Winkler, B. & Schnick, W. (2005). *Z. Kristallogr.* **220**, 245–249.
Hampshire, S. (1994). *Materials Science and Technology*, edited by R. W. Cahn, P. Haasen & E. J. Kramer, Vol. 11, pp. 119–171. Weinheim: VCH.
Hazen, R. M. & Finger, L. W. (1982) *Comparative Crystal Chemistry*. New York: Wiley-Interscience Publications.
Irran, E., Köllisch, K., Leoni, S., Nesper, R., Henry, P. F., Weller, M. T. & Schnick, W. (2000). *Chem. Eur. J.* **6**, 2714–2720.
Lieb, A., Weller, M. T., Henry, P. F., Niewa, R., Pöttgen, R., Hoffmann, R.-D., Höfer, H. E. & Schnick, W. (2005). *J. Solid State Chem.* **178**, 976–988.
Mao, H., Bell, P., Shaner, J. & Steinberg, D. (1978). *J. Appl. Phys.* **49**, 3276–3283.
Miletich, R., Allan, D. R. & Kuhs, W. F. (2000). *High-Temperature and High-Pressure Crystal Chemistry*, edited by R. M. Hazen & R. T. Downs, Vol. 41, pp. 445–520. Mineralogical Society of America Reviews in Mineralogy and Geochemistry.
Nordberg, L.-O., Nygren, M., Käll, P.-O. & Shen, Z. (1998). *J. Am. Ceram. Soc.* **81**, 1461–1470.
Robinson, K., Gibbs, G. V. & Ribbe, P. H. (1971). *Science*, **172**, 567–570.
Salje, E. K. H. (1990). *Phase Transitions in Ferroelastic and Co-elastic Crystals*. Cambridge University Press.
Schnick, W. (2001). *Int. J. Inorg. Mater.* **238**, 28–35.
Sheldrick, G. M. (1997*a*). *SHELXS*97. University of Göttingen, Germany.
Sheldrick, G. M. (1997*b*). *SHELXL*97. University of Göttingen, Germany.
Stokes, H. T. & Hatch, D. M. (1988). *Isotropy Subgroups of the 230 Crystallographic Space Groups*. Singapore: World Scientific Publishing Co. Pte. Ltd.
Thompson, D. P. & Mandal, H. (1996). *21st Century Ceramics*. London: The Institute of Materials.
Winkler, B., Hytha, M., Hantsch, U. & Milman, V. (2001). *Chem. Phys. Lett.* **343**, 622–626.